View metadata, citation and similar papers at core.ac.uk
brought to you by CORE
provided by UNT Digital Library

INL/CON-07-12639
PREPRINT

RCCS Experiments and Validation for High Temperature Gas-Cooled Reactor

NURETH-12

Chang Oh
Cliff Davis
Goon C. Park

September 2007

The INL is a
U.S. Department of Energy
National Laboratory
operated by
Battelle Energy Alliance

This is a preprint of a paper intended for publication in a journal or proceedings. Since changes may be made before publication, this preprint should not be cited or reproduced without permission of the author. This document was prepared as an account of work sponsored by an agency of the United States Government. Neither the United States Government nor any agency thereof, or any of their employees, makes any warranty, expressed or implied, or assumes any legal liability or responsibility for any third party's use, or the results of such use, of any information, apparatus, product or process disclosed in this report, or represents that its use by such third party would not infringe privately owned rights. The views expressed in this paper are not necessarily those of the United States Government or the sponsoring agency.

RCCS Experiments and Validation for High Temperature Gas-Cooled Reactor

Chang Oh* and Cliff Davis
Idaho National Laboratory
P.O. Box 1625
Idaho falls, ID 83415
Chang.Oh@inl.gov, Cliff.Davis@inl.gov,

Goon C. Park
Department of Nuclear Engineering
Seoul National University
Kwanak-Gu, Seoul, 151-742, Korea
parkc@snu.edu.re.kr

ABSTRACT

A reactor cavity cooling system (RCCS), an air-cooled helical coil RCCS unit immersed in the water pool, was proposed to overcome the disadvantages of the weak cooling ability of air-cooled RCCS and the complex structure of water-cooled RCCS for the high temperature gas-cooled reactor (HTGR). An experimental apparatus was constructed to investigate the various heat transfer phenomena in the water pool type RCCS. These included natural convection of air inside the cavity, radiation in the cavity, natural convection of water in the water pool, and forced convection of air in the cooling pipe.

The RCCS experimental results were compared with published correlations. The CFX code was validated using data from the air-cooled portion of the RCCS. The RELAP5 code was validated using measured temperatures from the reactor vessel and cavity walls.

KEYWORDS

Reactor cavity cooling for HTGR, RELAP5, and CFX

1. INTRODUCTION

A reactor cavity cooling system (RCCS) is equipped to remove the heat transferred from the reactor vessel to the structure of the containment. The RCCS are typically safety grade systems, either with passive or with high reliable, redundant forced-convection cooling system, designed to remove the entire core afterheat in the unlikely case of failure or unavailability of the main and all other shutdown cooling systems. The performance and reliability of the RCCS, therefore, are considered as the critical factors in determining maximum design power level related to afterheat removal. The over-designed capacity of the system, however, would not be acceptable

for the RCCS because during normal operation, and in some cases for normal shutdowns, excessive parasitic heat losses are undesirable. Also the fact that heat load distribution during long term loss of forced convection (LOFC) accidents can vary considerably with the accident characteristics make the design of the RCCS difficult. Due to the optimization difficulty of the RCCS capacity, experimental studies for the code validation and numerical studies using the validated codes are necessary to determine the adequacy of the design (IAEA-TECDOC-1163 2000 [1]). The characteristics of the RCCS in the HTGR under development are summarized in Table 1. In the high temperature engineering test reactor (HTTR), the first HTGR in Japan, the reactor cavity cooling is provided by forced convection of water along the cooling panel (Saito et al.1989 [2]). Two independent RCCSs named vessel cooling system (VCS) were equipped in the cavity. The heated water in the VCS is cooled by forced convection of water at the secondary side of the RCCS. The 10 MW High Temperature Gas-cooled Test Reactor (HTR-10) developed in China adopts two independent water cooled RCCSs which remove the after heat by natural circulation of water (Wu et al. 2002 [3]).

Table 1 RCCS types in HTGRs.

Reactor	**RCCS Coolant Type**	**Secondary Coolant Type**
HTTR	Water Forced Convection	Water Forced Convection
HTR-10	Water Natural Convection	Air Natural Convection
PBMR	Water Natural Convection	Air Natural Convection
GT-MHR	Air Natural Convection	No Secondary cooling
MHTGR	Air Natural Convection	No Secondary cooling

The water coolers are connected with the air coolers on the top of the reactor building located in the two chimneys. The air flow supplied by the chimneys removes the after heat to atmosphere. The RCCS of the 265 MW pebble bed modular reactor (PBMR) developed in South Africa includes three independent systems each consisting of a natural convection driven water cooling system with passive external water-to-air heat exchanger (IAEA-TECDOC-1198 2001 [4]). In the case where all the cooling units failed, the heat of the reactor is absorbed by heating up and then boiling off the water in the system. The systems are sized to provide this cooling function for up to three days. The gas turbine modular helium reactor (GT-MHR) has 600 MW thermal power and is planned to be constructed in Russia (IAEA-TECDOC-1198 2001 [4]). The RCCS of the GT-MHR removes heat by conduction through the graphite reflector and by radiation and natural convection from the uninsulated vessel. The system, which receives the heat transferred from the vessel, includes a cooling panel placed around the reactor vessel. Heat is removed from the reactor cavity by natural circulation of outside air through the cooling panel. The 450 MW

modular high temperature gas-cooled reactor (MHTGR) developed in the United States has an air cooled RCCS which rejects the after heat to the atmosphere by buoyancy-driven natural circulation of outside air through the cooling panels (Dilling et al. 1982 [5]). The system should function during all period of normal operation and accidents and does not rely on any active component or operation action.

As summarized in Table 1, the cooling capability of the RCCS in the developed HTGR is provided by forced convection of water, natural circulation of water or natural circulation of air. It was reported that the active water cooling RCCS has efficient cooling capability and is easy to design comparing with the others. However it has the possibility of over-cooling as well as the very complex features to provide the same level of reliability as the passive cooling scheme. The passive water cooling RCCS can reject the after heat efficiently with high reliability but needs complicated structures and affiliated systems such as secondary side cooling system and water purification system. It was also reported that there is significant uncertainty and complexity associated with two-phase phenomena in the boiling mode for the water cooling scheme (Dilling et al. 1982 [5]). The air cooling scheme has fewer failure modes and is more passive than the others but it was known to be difficult to design because the air flow around the reactor pressure vessel (RPV) is deviated due to the effects of nozzle locations (IAEA-TECDOC-1163 2000 [1]). Also due to poor cooling capability of natural circulating air, a very high chimney is necessary to supply enough air flow to remove the after heat.

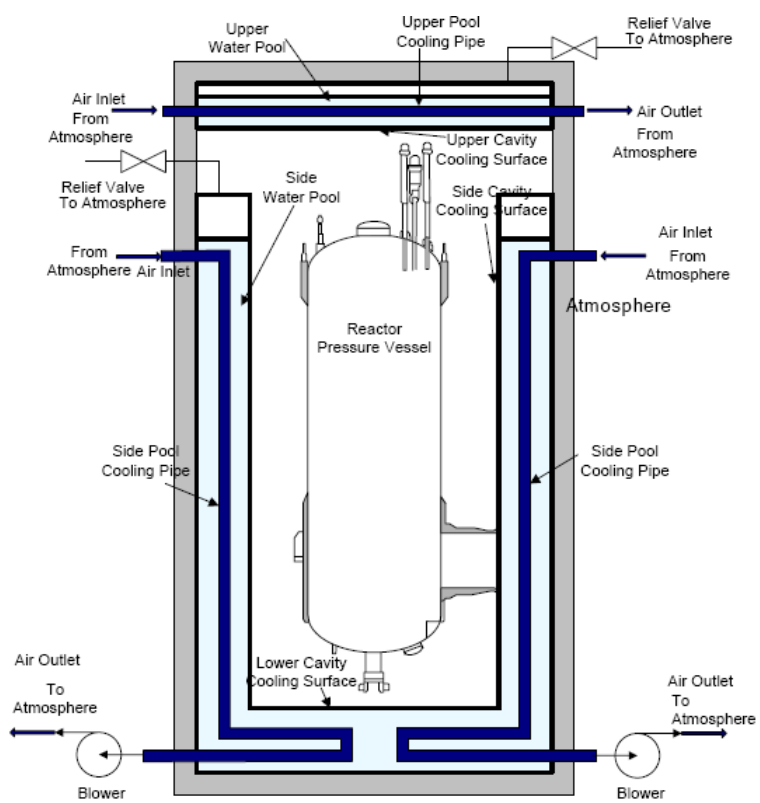

Figure 1. RCCS system configuration (Side View).

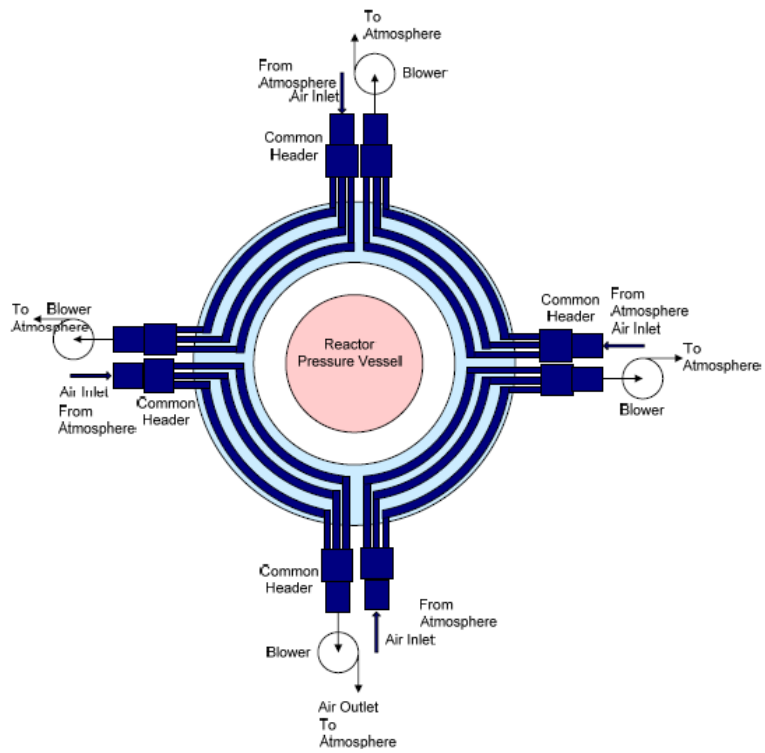

Figure 2. Top view of the water pool type RCCS.

2. EXPERIMENTS

An experimental apparatus was constructed to investigate the various heat transfer phenomena in the water pool type RCCS, such as the natural convection of air inside the cavity, radiation in the cavity, the natural convection of water in the water pool and the forced convection of air in the cooling pipe. The schematic diagram and the photos of the experimental apparatus are shown in Figures 3 and 4.

The apparatus mainly consists of a reactor vessel, a side water pool surrounding the vessel, an upper water pool, cooling pipes in the water pools and air supply systems. The reactor vessel of the test facility is a 1/10 linear scaled model of the PBMR (265 MW). In the reactor vessel, six heaters were installed to simulate the heat loss which occurs during normal operation and the afterheat during an LOFC accident. The heat released from the reactor vessel is transferred to the side pool and the upper pool through the cavity by radiative and natural convective heat transfer. To remove the heat, thirteen cooling pipes are installed in the side pool and the upper pool (12 in the side pool, one in the upper pool) as shown in Figure 5 (a and b). Three of the cooling pipes within the same quarter section of the side pool are contained in one train of the RCCS. The outlets of the cooling pipes are connected to common headers, and each common header is connected to a suction of the blowers. Ambient air enters into the inlet of the cooling pipes and enables the heat from the side pool and the upper pool to be released to the atmosphere. During both normal operation and accident conditions, the steam generated by evaporation or boiling in the water pools is vented to the atmosphere through the relief valves which are opened at 1.5 bars.

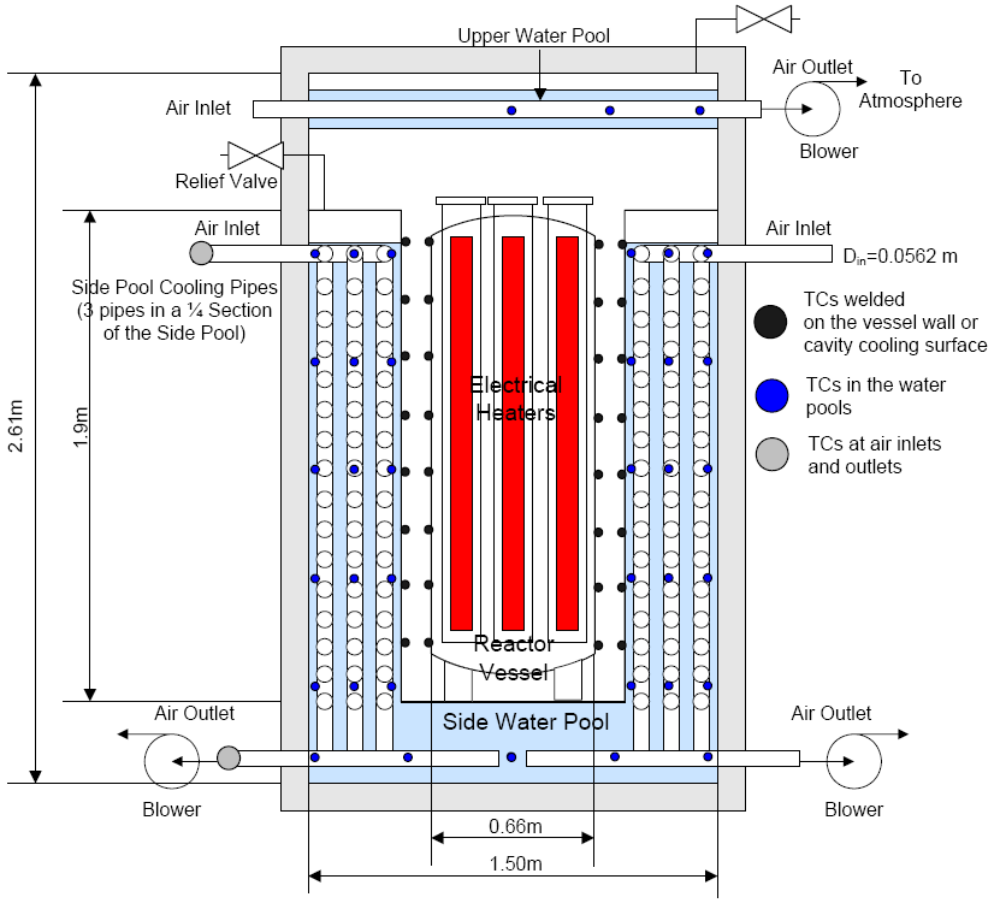

Figure 3. Schematic diagram of the test facility.

Figure 4. Photograph of the test facility.

(a) Upper tank (b) Water tank

Figure 5. Configuration of the cooling pipe.

The major measurement parameters are the air flow rates, the pressure drops along the cooling pipes, the water level in the side pool, the pressures in the water pools, reactor vessel and cavity, and the temperatures. The location of the thermocouples is presented in Figure 3. The temperatures of the water pool were measured at three radial positions, five axial positions and three azimuthal positions, and four additional thermocouples were installed at the bottom of the water pool and at the water level elevation. A total of 48 thermocouples were welded to the wall of the reactor vessel and the cavity. The flow rates of air were measured by means of thirteen average bi-directional flow tubes located at each inlet of the cooling pipes (Yun et al. 2004 [6]) and the water level in the side pool was measured by means of a differential pressure transmitter.

3. HEAT TRANSFER ANALYSIS

From the experimental results the heat transfer coefficient at inner surface of cooling pipe for the forced convection was calculated.

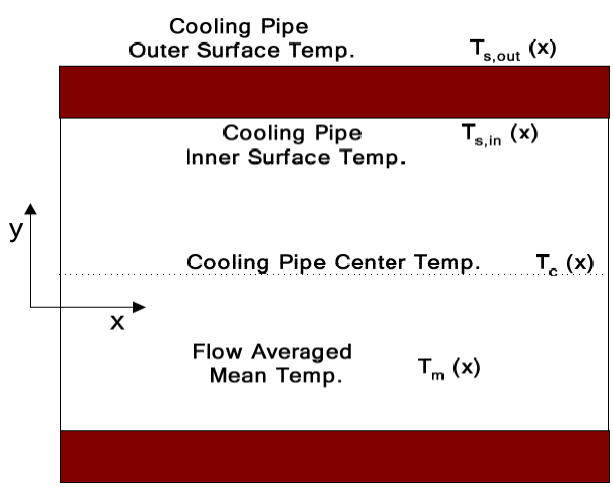

Figure 6. Control volume of the cooling pipe.

Applying conservation of energy, Eq. (1), to the differential control volume of Figure 6, we obtain

$$d\dot{q}_{conv} = \dot{m}_g c_p dT_m = 2\pi h r_{in} dx \left(T_{s,in} - T_m\right) \quad \text{or} \quad h = \frac{\dot{m}_g c_p}{2\pi r_{in}} \frac{dT_m}{dx} \frac{1}{T_{s,in} - T_m} \tag{1}$$

The flow averaged mean temperature and pipe inner surface temperature in above equation should be substituted by the temperature of the cooling pipe center and outer surface that were measured in the experiments to calculate the heat transfer coefficient. Since information for the velocity and temperature fields of the cooling pipe is necessary to obtain the mean temperature, we assumed that those are the same with the velocity and temperature profiles of the fully developed turbulent flow under the constant temperature condition. The appropriateness of this assumption will be discussed with a calculation result using the CFX code [7] later. Applying the assumption, the flow averaged mean temperature can be expressed as follows.

$$T_m = \frac{3}{2(n+2)} T_{s,in} + \frac{2n+1}{2(n+2)} T_c \quad \text{(where, n=7) (Kakac et al., 1987 [8])} \tag{2}$$

In Figure 6, the heat transfer in the cooling pipe by conduction can be expressed as,

$$d\dot{q}_{cond} = \frac{2\pi dxk\left[T_{s,out} - T_{s,in}\right]}{\ln\left(r_{out}/r_{in}\right)} \tag{3}$$

Equating Eq.(1) and Eq.(3) it follows that the derivative of the mean temperature is related to the temperatures at the cooling pipe inner and outer surface.

$$\frac{dT_m}{dx} = \frac{2\pi k}{\dot{m}_g c_p} \frac{\left[T_{s,out} - T_{s,in}\right]}{\ln\left(r_{out}/r_{in}\right)} = \frac{2\pi h r_{in}}{\dot{m}_g c_p}\left[T_{s,in} - T_m\right] = \frac{2\pi h r_{in}}{\dot{m}_g c_p}\left[T_{s,in} - T_c\right]\frac{2n+1}{2(n+2)} \tag{4}$$

Rearranging Eq.(4), we obtain Eq. (5)

$$\frac{k(T_{s,out} - T_{s,in})}{\ln(r_{out}/r_{in})} = h r_{in}(T_{s,in} - T_c)\frac{2n+1}{2(n+2)} \quad \text{or} \quad T_{s,in} = \frac{\dfrac{kT_{s,out}}{\ln(r_{out}/r_{in})} + h r_{in} T_c \dfrac{2n+1}{2(n+2)}}{h r_{in}\dfrac{2n+1}{2(n+2)} + \dfrac{k}{\ln(r_{out}/r_{in})}} \tag{5}$$

Substituting from Eq.(5), Eq.(1) and Eq. (4) can be expressed as follows,

$$h = \frac{\dot{m}_g c_p}{2\pi r_{in}} \frac{dT_m}{dx} \frac{2(n+2)}{2n+1} \frac{1}{\dfrac{\dfrac{kT_{s,out}}{\ln(r_{out}/r_{in})} + h r_{in} T_c \dfrac{2n+1}{2(n+2)}}{h r_{in}\dfrac{2n+1}{2(n+2)} + \dfrac{k}{\ln(r_{out}/r_{in})}} - T_c} \tag{6}$$

$$\frac{dT_m}{dx} = \frac{3}{2(n+2)}\frac{dT_{s,in}}{dx} + \frac{2n+1}{2(n+2)}\frac{dT_c}{dx} \tag{7}$$

$$= \frac{2n+1}{2(n+2)}\frac{dT_c}{dx} + \frac{3}{2(n+2)}\left[\frac{\frac{k}{\ln(r_{out}/r_{in})}\frac{dT_{s,o}}{dx} + r_{in}\frac{2n+1}{2(n+2)}\left[\frac{T_c dh}{dx} + \frac{h dT_c}{dx}\right]}{\frac{k}{\ln(r_{out}/r_{in})} + hr_{in}\frac{2n+1}{2(n+2)}} - \frac{\left(\frac{kT_{s,o}}{\ln(r_{out}/r_{in})} + hr_{in}T_c\frac{2n+1}{2(n+2)}\right)\cdot\frac{2n+1}{2(n+2)}r_{in}\frac{dh}{dx}}{\left(\frac{k}{\ln(r_{out}/r_{in})} + hr_{in}\frac{2n+1}{2(n+2)}\right)^2}\right]$$

The spatial derivatives of the temperature at the outer surface and axis of the pipe in Eq. (7) can be obtained from the experimental data with the multiple regression method. Assuming the spatial distribution of the heat transfer coefficient to a third order polynomial, we can solve Eqs. (6) and (7) at each measuring location. Excluding the effect of conduction, Eq.(6) can be reduced as follows,

$$h = \frac{\dot{m}c_p}{2\pi r_{in}}\frac{1}{T_s - T_c}\frac{2(n+2)}{2n+1}\frac{dT_m}{dx} = \frac{\dot{m}c_p}{2\pi r_{in}}\frac{1}{T_s - T_c}\frac{2(n+2)}{2n+1}\left[\frac{3}{2(n+2)}\frac{dT_s}{dx} + \frac{2n+1}{2(n+2)}\frac{dT_c}{dx}\right] \tag{8}$$

Integrating above equation along the axis, we can obtain averaged heat transfer coefficients.

$$\bar{h} = \frac{1}{L}\int_0^L h dx = \frac{\dot{m}c_p}{2\pi rL}\frac{2(n+2)}{2n+1}\int_0^L \frac{1}{T_s - T_c}\left[\frac{3}{2(n+2)}\frac{dT_s}{dx} + \frac{2n+1}{2(n+2)}\frac{dT_c}{dx}\right]dx \tag{9}$$

In Figure 7, the calculation results of the Nusselt number in the cooling pipe were indicated and compared with correlations of previous studies to evaluate the correlations. The Dittus-Boelter correlation (Dittus and Boelter, 1930 [9]) for fully developed turbulent flow and the Mori-Nakamura correlation (Mori and Nakayama, 1967 [10]) for a helical coil which is implemented in RETRAN3D/INT (Paulsen et al, 1996 [11]) were used for the evaluation. In comparison, our experimental data was found to be 30% higher than the predicted curve by Dittus-Boelter for a straight pipe because of the effect of secondary flow in curved pipes. Also the Nusselt numbers are about 10 % larger for the cooling pipe than for a helical coil tube which has the same radius (r_{coil}=0.5m) with our test facility. This underestimation seems to have been caused by the presence of the U-bend. Tailby and Staddon (1970 [12]) reported Nusselt number increments for air cooling in 180° bend. They explained that in a bend secondary flow pushes heavier fluid particles toward the outer wall and lighter ones toward the inner wall and thus the bend augments the secondary flow resulting in significantly higher heat transfer coefficients at the outer wall. Also Moshfeghhian and Bell (1979) [13] observed higher heat transfer coefficient in the downstream of the bend as well as in the bend.

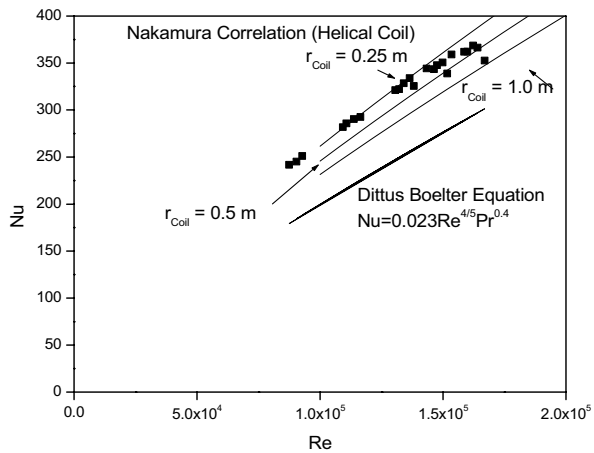

Figure 7. Averaged heat transfer coefficient.

From this characteristic of the heat transfer phenomena in the cooling pipe, a CFX calculation was carried out to obtain detailed information of the fluid velocity and temperature. The calculation simulates the cooling pipe alone and the experimental data of the cooling pipe surface temperature were implemented as boundary conditions. The k-ε model was used for turbulent modeling. Figure 8 shows the grid and velocity vectors of the calculation. Figures 9 and 10 show the calculation results of the velocity and temperature profiles at the temperature measuring locations of the cooling pipe. The centrifugal effect of the bend, which shifts the maximum of the axial velocity toward the outer wall, is well represented in our calculation as shown in Figure 11. This is the same trend with the results of Pruvost et. al. (2004) [14] who investigated the flow structure in U-bend using the FLUENT [15]. Also our calculation result for the air temperature at the axis showed a reasonably good agreement with the experimental data. From this calculation results, we concluded that the CFX code can simulate the heat transfer phenomena in the cooling pipe of SNU-RCCS.

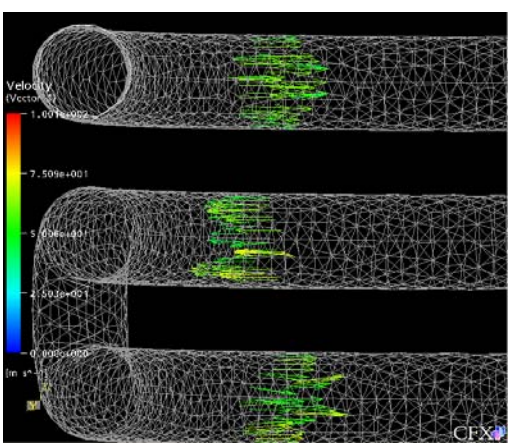

Figure 8. CFX grids and velocity vectors.

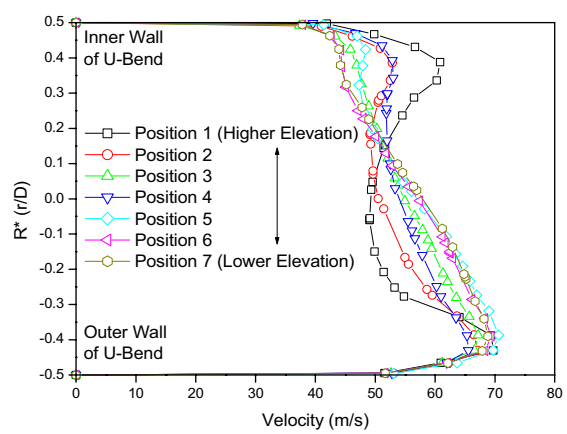

Figure 9. CFX velocity profiles

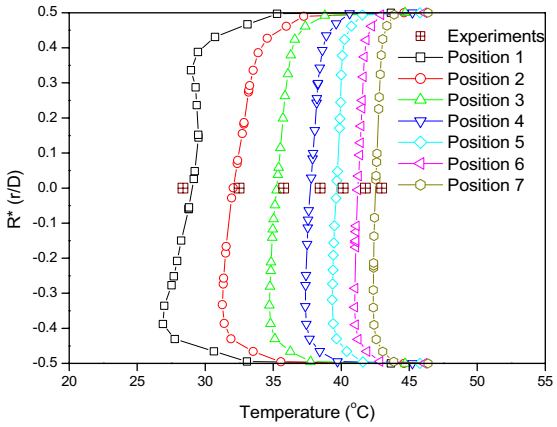

Figure 10. CFX temperature profiles.

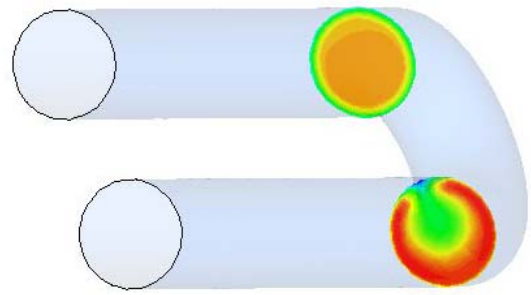

Figure 11. Velocity at the U-bend

4. RELAP5 Validation

The RELAP5-3D code (INEEL 2005) [16] was assessed using an experiment from Seoul National University (SNU) (V30Q25) that simulated multi-dimensional heat conduction through a reactor vessel (RV) and heat transfer to a surrounding cavity wall (CW). Note that the RCCS was located outside of the cavity wall and was not modeled explicitly in this calculation.

The RELAP5-3D model of the SNU experiment is illustrated in Figure 12. The RV was modeled as a solid circular cylinder with a radius and height of 410 and 1585 mm, respectively. The RV contained six 90-mm diameter heater rods centered at a radius of 225 mm and spaced uniformly in the azimuthal direction. The power applied to the heater rods was 25 kW. The power was conducted from the heater rods to the various surfaces of the RV, where it was transferred to the CW through radiation and convection. Some of the power was also conducted through the support legs of the reactor vessel to the lower wall of the cavity. Most of the outer surface of the CW was cooled with water. Temperature measurements were taken at various locations on the cavity and vessel walls.

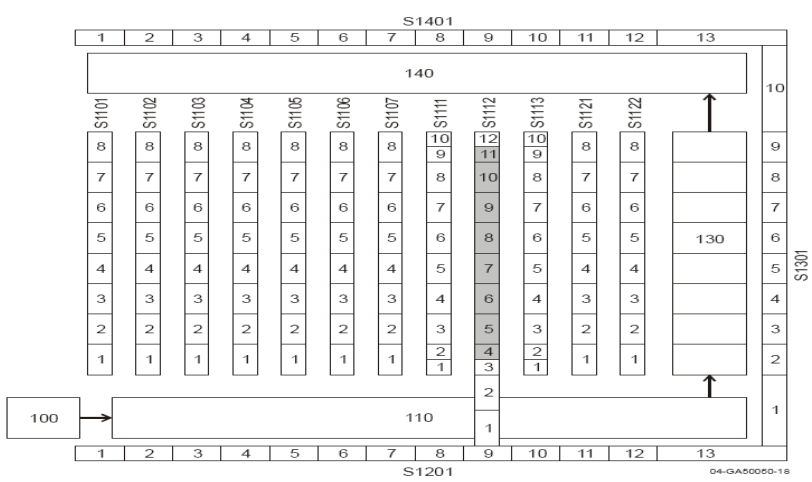

Figure 12. RELAP5-3D model of the SNU RCCS experiment.

The RV was modeled with a two-dimensional mesh with 12 radial rings and at least 8 axial segments. The inner and outer rings were represented with Structures 1101 and 1122, respectively. Structure 1112 represented the heater rods. The thickness of this structure preserved the volume of the heater rods. A uniform volumetric heat generation rate was applied to the active section of the heater rods (Segments 4 through 11). The RV was modeled as CA508 carbon steel. The CW was modeled as SS304 stainless steel.

The multi-dimensional heat conduction through the RV was approximated using a conduction enclosure model. Each heat structure communicated thermally with the adjacent heat structures in both the radial and axial directions. The support legs were modeled below the heater rods and were assumed to have the same thickness. The outer ring of the RV was coupled to the vertical CW through a radiation enclosure model. Free convection heat transfer coefficients were applied to the upper, lower, and vertical surfaces of the RV and the inner walls of the cavity. The code's default correlations were applied to the vertical surfaces. Correlations for isothermal heated and cooled plates (Holman 1986) were applied at the top and bottom of the reactor vessel and the horizontal surfaces of the CW. Temperature boundary conditions were applied to the outside surfaces of the CW heat structures (S1201, S1301, and S1401). These temperatures were 28 °C and 207 °C for Structures 1201 and 1401, respectively. The temperatures applied to the outside surface of the Structure 1301 were a function of elevation.

A simple, one-dimensional hydrodynamic model was used to simulate the air spaces surrounding the RV. The gaps represents by Components 110, 130, and 140 were 200, 90, and 370 mm thick, respectively. A time-dependent volume (Component 100) was used to maintain the pressure at 0.13 MPa. The temperature profiles in the experiment would induce multi-dimensional natural circulation patterns within the horizontal and vertical sections, but such patterns cannot be predicted with the simple, one-dimensional model used here. The multi-dimensional flow patterns were neglected for this analysis, and the free convection heat transfer correlations were relied upon to calculate the heat transfer between the walls and the fluid.

The code's enclosure models have several limitations for modeling a complicated geometry such as involved in the SNU experiment. First, the gap conductance in the conduction model and the emissivity in the radiation model are treated as constants for each surface, whereas they actually depend on temperature. For this analysis, the gap conductances in the axial direction were based on a thermal conductivity of 45 W/m-K. The gap conductances in the radial direction were set to a large value because the thermal resistance within each heat structure was already accounted for with the code's one-dimensional heat conduction model. The emissivities of the RV and CW were set to 0.8 and 0.6, respectively, based on measurements. Second, and more serious, the heat conduction model is based on a one-dimensional formulation in which each structure has only two surfaces, instead of the six surfaces actually present. Each surface can be included in only one enclosure model. For this analysis, all the RV surfaces were utilized for radial and axial conduction except for the outer surface of S1122, which was utilized for radiation to the vertical CW. Consequently, no surfaces were available to account for radiation between the upper and lower faces of the RV and the horizontal walls of the cavity. The radiation from these faces was simulated through the use of enhanced convection to the fluid. The radiation heat transfer between walls was converted to an equivalent heat transfer coefficient to the fluid and then added to the coefficient obtained for free convection as described previously. A combined

heat transfer coefficient was then applied to both the RV and CW surfaces that preserved the total heat transfer between surfaces. Finally, the input required for the conduction enclosure model is more complicated to generate than would be required with a true two-dimensional heat conduction model. The results of the assessment using the SNU RCCS experiment are shown in Figure 13. The figure presents calculated and measured temperatures of the CW and RV as a function of height above the lower CW. Scatter in the measured values reflects azimuthal temperature variation at a given height. There is no corresponding scatter in the calculated results because the heat conduction model was two-dimensional rather than three-dimensional. The increase in the CW temperature near 1.6 m reflects the location of the liquid level on the outside of the wall. CW temperatures were input to the model as boundary conditions.

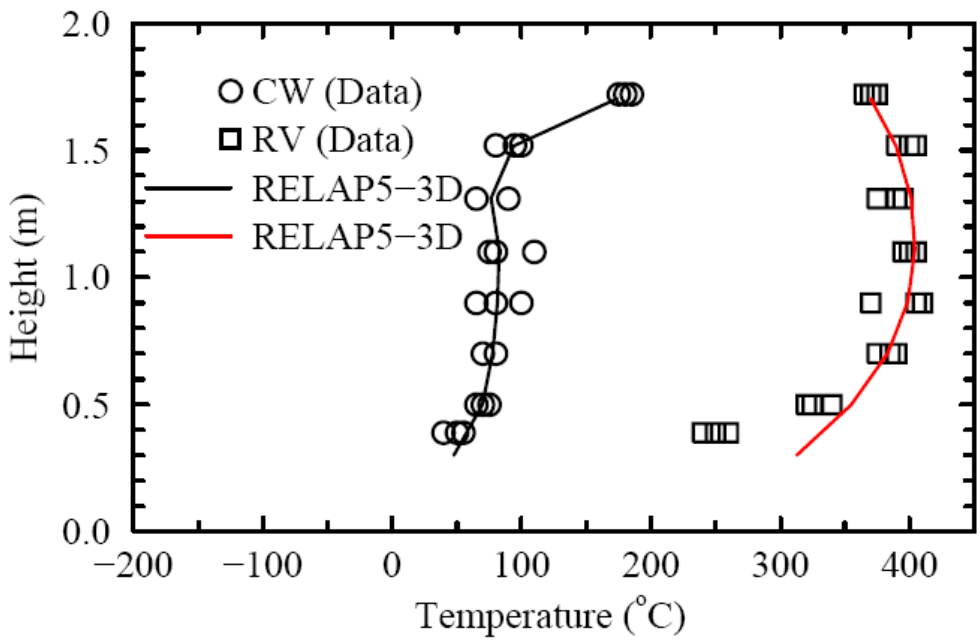

Figure 13. A comparison of calculated and measured temperatures for the SNU RCCS experiment.

The calculated RV wall temperatures were in reasonable agreement with the measured values. The maximum predicted value occurred slightly above the centerline of the heated length and was in excellent agreement with the maximum measured value. The code's prediction of the temperature decrease near the top of the vessel was also in excellent agreement with the test. A larger decrease occurred near the bottom of the RV in both the calculation and the experiment because of the heat loss through the support legs of the vessel and because of the smaller sink temperature applied to the lower CW. The magnitude of the temperature decrease near the bottom of the RV was larger in the experiment than in the calculation. The results obtained with RELAP5-3D are similar to those obtained previously with the GAMMA code [17]. Possible causes for the discrepancy include the lack of modeling of the bottom insulation plug of the heater element and the lack of detailed information about the geometry of the support legs.

An evaluation of the calculated results showed that radiation from the vertical wall of the RV to the CW accounted for about 60% of the total power. Convection between the vertical walls accounted for an additional 20% of the power. Conduction through the support legs accounted for about 10% of the power while radiation and convection from the lower and upper faces accounted for the remainder.

5. CONCLUSIONS

A new kind of RCCS, water pool type RCCS was proposed to overcome the disadvantages of the weak cooling ability of air-cooled RCCS and the complex structure of water-cooled RCCS. The feasibility of the system was estimated by a series of experiments. The experimental results were used to validate the CFX code.

The RV temperature profile calculated by RELAP5-3D was in reasonable agreement with the measurements from the RCCS experiment, even with the simple, one-dimensional hydrodynamic model and the noted limitations in the code's enclosure models.

ACKNOWLEDGMENTS

This work was supported through the Department of Energy's International Nuclear Energy Research Initiative Project NE-INERI-2002-001 under DOE Idaho Operations Office Contract DE-AC07-99ID13727.

REFERENCES

1. IAEA, 2000, Heat Transport and Afterheat Removal for Gas Cooled Reactors under Accident Conditions, IAEA-TECDOC-1163, Vienna.
2. Saito et al., 2000, Design and Safety Consideration in the High-Temperature Engineering Test Reactor (HTTR), IAEA-TC-389, Dimitrovgrad.
3. Wu et al., 2002, "The Design Features of the HTR-10," Nuclear Engineering and Design, Vol. 218, pp. 25-32.
4. IAEA, 2001, Current Status and Future Development of Modular High Temperature Gas Cooled Reactor Technology, IAEA-TECDOC-1198.
5. Dilling D.A. et al., 1982, Passive Decay and Residual Heat Removal in the MHTGR, IAEA-TECDOC-757, Juelich.
6. Yun B. J. et al., 2004, "Measurement of the Two-phase Mass Flow Rate Using an Average Bidirectional Flow Tube," Proceeding of Two-Phase Flow Modeling and Experimentation, Pisa, Italy, September.
7. AEA Technology Engineering Software, CFX-5.
8. Kakac S., Yener Y., Convective Heat Transfer, CRC Press, 1994, pp. 147
9. F.W. Dittus and L.M.K. Boelter, University of California, Berkeley, Publications on Engineering, Vol.2, p 443, 1930.
10. Mori Y. and Nakayama W. , 1967, "Study on Forced convective Heat Transfer in Curved Pipes," Int. J. Mass Transfer, 10, pp. 37-59.

11. Paulsen, et al., “RETRAN-3D – A Program for Transient Thermal-Hydraulic Analysis of Complex Fluid Flow Systems,” EPRI NP-7450, 1996.
12. Tailby S. R. and Staddon P.W., 1970, "The Influence of 90o and 180o Pipe Bends on Heat Transfer from an Internally Flowing Gas Stream," Heat Transfer, Vol.2 paper No. FC 4.5.
13. Moshfeghian M. and Bell K.J., 1979, "Local Heat Transfer Measurements in and Downstream from a U-bend," ASME paper No. 79-HT-82.
14. Pruvost J.,J.Legrand and P.Legentilhomme, “Numerical investigation of bend and torus ows,part I :effect of swirl motion on structure in U-bend,” *Chemical Engineering Science*, **59**, pp. 3345 –3357, 2004.
15. Fluent Inc., Fluent User’s Manual version 5.1998.
16. INEEL, 2005, RELAP5-3D Code Manual, INEEL-EXT-98-00834, Revision 2.3, April 2005.
17. Oh et. al., Development of Safety Analysis Codes and Experimental Validation for a Very High Temperature Gas-Cooled Reactor, INL/EXT-06-01362, March 2006.